COMPUTER METHODS AND PROGRAMS IN BIOMEDICINE 96 (2009) 85–95

journal homepage: www.intl.elsevierhealth.com/journals/cmpb

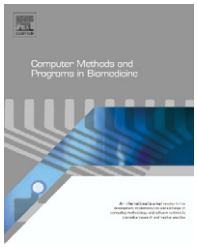

Detection of blood vessels in ophthalmoscope images using MF/ant (matched filter/ant colony) algorithm

Muhammed Gökhan Cinsdikici[a,*], *Doğan Aydın*[b]

[a] *Ege University Int'l Computer Institute, Bornova 35100, İzmir, Turkey*
[b] *Ege University Computer Engineering Department, Bornova 35100, İzmir, Turkey*

ARTICLE INFO

Article history:
Received 19 February 2009
Received in revised form
19 February 2009
Accepted 6 April 2009

Keywords:
Retinal (Ophthalmoscope) image
blood vessel segmentation
Matched filter
Ant algorithm
DRIVE database

ABSTRACT

Blood vessels in ophthalmoscope images play an important role in diagnosis of some serious pathologies on retinal images. Hence, accurate extraction of vessels is becoming a main topic of this research area. Matched filter (MF) implementation for blood vessel detection is one of the methods giving more accurate results. Using this filter alone might not recover all the vessels (especially the capillaries). In this paper, a novel approach (MF/ant algorithm) is proposed to overcome the deficiency of the MF. The proposed method is a hybrid model of matched filter and ant colony algorithm. In this work, the accuracy and parameters of the hybrid algorithm are also discussed. The proposed method shows its success using the well known reference ophthalmoscope images of DRIVE database.

1. Introduction

Segmentation of blood vessels in ophthalmoscope images plays an important role in diagnosis of some serious pathologies like diabetes, glaucoma and hypertension.

Since illumination, geometry and reflectance properties vary image by image, accurate vessels extraction takes critical role. The other factors affecting the segmentation can be summarized as presence of noise, low contrast between background and vessel regions, vessel widths, lesions over the interested area and exudates.

The methods for extracting blood vessels proposed in literature are mainly based on kernel-based, classifier-based and tracking-based approaches [1].

In kernel-based methods [2,3], a Gaussian shaped curve models the cross-section of a vessel and detects vessels using rotated matched filters.

Classifier-based methods [4–6] are given in two steps: first, a segmentation of spatially connected regions is produced by a low-level algorithm. Then blood vessels are detected by classification of these candidate regions according to many features.

Tracking-based methods [7–9] start locating interested vessel points for tracing, and then segment the vessels according to some local image features.

Ant-based approaches, inspired from real ant colonies, are becoming state-of-the-art in image segmentation. They are going to be popular in edge detection [10,11], histogram thresholding, and clustering.

Nezamabadi-pour et al. applied an ant-based approach to detect edges [10]. In their method, candidate edge fields are wandered by ants according to probabilistic translation decision rule and ants deposit some amount of pheromones indicating the likelihood of the pixel belongs to an edge field.

* *Corresponding author*. Tel.: +90 232 342 3232x129.
E-mail address: muhammed.cinsdikici@ege.edu.tr (M.G. Cinsdikici).
0169-2607/$ – see front matter © 2009 Elsevier Ireland Ltd. All rights reserved.
doi:10.1016/j.cmpb.2009.04.005

In histogram thresholding, ant-based approaches are used to find optimum threshold values and some different implementations can be found in [12–15].

The clustering by ant algorithms is examined in to two ways [16]. First, for those directly mimics real ant colonies, the clustering behaviors can be seen as patch sorting and annual sorting [17–20]. Other is examined as heuristics reformulating the clustering problem as an optimization task [21,22]. Besides, hybridized methods were also presented in [23–25].

In this paper, a hybrid model of ant-based clustering and MF algorithms is introduced. Although ant-based algorithms or MF algorithms are sufficient to extract blood vessels, using the hybrid form can improve the accuracy and false/true ratios performance of the resultant images. In Section 2, definitions and design considerations of ant, MF and our proposed MF/ant algorithms are given. Section 3 demonstrates the experimental results. In the final section, our proposed algorithm is discussed and concluded.

2. Materials and methods

2.1. *Ant algorithms*

Ant algorithms based on the foraging behavior of ants have first been introduced by Dorigo et al. in [26–28] and were formalized as a new meta-heuristic in [29] by Dorigo and Di Caro.

In ant algorithms, a number of artificial ants build solutions to the considered optimization problem at hand and exchange information on the quality of these solutions via a communication scheme that is reminiscent of the one adapted by real ants [30]. The skeleton of ant algorithms is shown below:

```
Procedure Ant algorithm
  Set parameters, initialize pheromone trails
    while (termination condition not met) do
      ConstructSolutions
      ApplyLocalSearch % optional
      UpdateTrails
    end
end Ant algorithm
```

As seen from algorithm that there are four steps of the algorithm: Preprocessing, Solution Construction, Local Searching and Pheromone Updating. They are described as follows:

Preprocessing: The parameters of the ant algorithm such as the number of ants, iteration and memory sizes are initialized according to priori-knowledge obtained from empirical data. Besides, pheromone trails are also initialized with small numbers (i.e. $<10^{-5}$) [31].

ConstructSolutions: For the given problem instance, each ant starts with a random state then traverses the states one by one according to the probability distribution function. Each ant chooses its new state through the comparison of its random threshold value with the produced probabilities of states primarily defined by the Eq. (1). This random selection is called "*random proportional transition rule* (RPT)" [31] (also called as pseudo-random proportional rule) and depends on the combination of two values:

- *Attractiveness* of the move (i.e. visibility), is a heuristic function (that is depends on the problem) indicating the priori desirability of that move.
- The *trail level* of artificial pheromone, indicates posteriori desirability of the move based on learned (i.e. historical) experiences. In other words trail level indicates the awareness level of the candidate state.

The first ant algorithm, ant system (AS) [28], defines the RPT rule as in Eq. (1);

$$P_{ij} = \begin{cases} \dfrac{[\tau_{ij}]^{\alpha}[\eta_{ij}]^{\beta}}{\sum_{h\in\Omega}[\tau_{ih}]^{\alpha}[\eta_{ih}]^{\beta}} & \text{if} \quad j \in \Omega \\ 0 & \text{otherwise} \end{cases} \tag{1}$$

where τ_{ij} is intensity of trail between states i and j, η_{ij} is visibility of state j from state i (η_{ij} changes according to the problem definition), Ω is the set of unvisited states and finally, α and β are two adjustable parameters that affect the algorithm performance.

All ant algorithms except ant colony system (ACS) [32] use the same RPT rule. In ACS, it is modified to allow explicitly for exploration as follows:

$$j = \begin{cases} \arg\ \max\limits_{j\in\Omega} \left\{ \tau_{ij}\eta_{ij}^{\beta} \right\} & \text{if} \quad q \le q_0 \\ J & \text{otherwise} \end{cases} \tag{2}$$

where q_0 is a controller parameter for the exploration and is a constant ($0 \le q_0 \le 1$) assigned at the preprocessing level. q is a uniformly distributed random number determined at each move (i.e. transition from the state i to state j). J is the previous probability distribution function given in Eq. (1). If $q \le q_0$ then the best state is chosen (exploitation), otherwise a state is chosen according to Eq. (1) (biased exploration) [33].

ApplyLocalSearch: Before updating trail levels, local search methods can be applied on each solution constructed in current iteration. Although this process is optional and problem specific, it improves the solutions obtained by the ants and has been used by state of art ant algorithms.

UpdateTrails After the solutions constructed and calculated, pheromone levels on paths increase (pheromone depositing) and decrease (pheromone evaporation) related to the better and worse solutions respectively.

Indirect multiple communication of the colony is provided by the positive and negative feedbacks of the pheromone updates. Positive feedback is implemented by pheromone laying on the better solutions for reinforcement. Unfortunately, increasing pheromone level without evaporation leads the stagnation state. To avoid this, negative feedback mechanism is introduced through the pheromone evaporation.

In AS, every ant deposits certain amount of pheromone depicted in Eq. (3) at the end of each iteration.

$$\text{Pheromone} = \frac{1}{L_k} \tag{3}$$

In (3) "k" represents the ant and L_k is the cost of the tour (i.e. path) completed by that ant.

After depositing accomplished, pheromone level of every edges decreased by the Eq. (4) where constant ρ ($0 \le \rho \le 1$) is the coefficient of decay determined at the beginning of the algorithm.

$$\tau_{ij}(t+1) = (1-\rho)\tau_{ij}(t) \tag{4}$$

In ACS, two types of pheromone updating strategies are used: Local and global.

In global updating, after each iteration, only the pheromones on globally best path (gbp) are updated by increasing pheromone level of Eq. (5);

$$\tau_{ij}(t+1) = (1-\rho)\tau_{ij}(t) + \frac{\rho}{L_{gbp}} \tag{5}$$

where ρ is the decay parameter mentioned for AS.

In local updating, the pheromone level of the current state is modified by the Eq. (6) before visiting to the next state in a tour.

$$\tau_{ij} = (1-\varphi)\tau_{ij} + \varphi\tau_0 \tag{6}$$

where constant φ ($0 < \varphi \le 1$) is the local pheromone decay coefficient and τ_0 is the initial value of the pheromone.

2.2. *Matching filters (MF)*

Designing MF for ophthalmoscope images is based on number of properties for blood vessels;

a. Blood vessel shapes shows small curvatures, so anti-parallel pairs may be approximated.
b. Vessels are observed as darker areas compared with background.
c. Vessel widths are ranged in 2–20 pixels

Retinal images are convolved with the MF through the following steps;

a. Green Channel of the image is extracted to be processed.
b. Rotation matrix is defined as in Eq. (7);

$$r = \begin{bmatrix} \cos\theta_i & -\sin\theta_i \\ \sin\theta_i & \cos\theta_i \end{bmatrix} \tag{7}$$

c. Construct MF kernels spanning possible orientations with the rotation matrix. (θ is changed with predefined angle). In Eq. (8), N indicates the neighborhood defined in the area of [u,v] where $|u| \le 3\sigma$ and $|v| \le L/2$ [2]. L is used as kernel size of priori information about vessel length. So the new coordinate calculated with multiplication of Kernel by the transpose of rotation matrix [2].

$$\begin{aligned} \tilde{p}_i &= \begin{bmatrix} u & v \end{bmatrix} = K(x,y) * r^T \\ K_i(x,y) &= -\exp^{(-u^2/2\sigma^2)} \quad \forall \tilde{p}_i \in N \end{aligned} \tag{8}$$

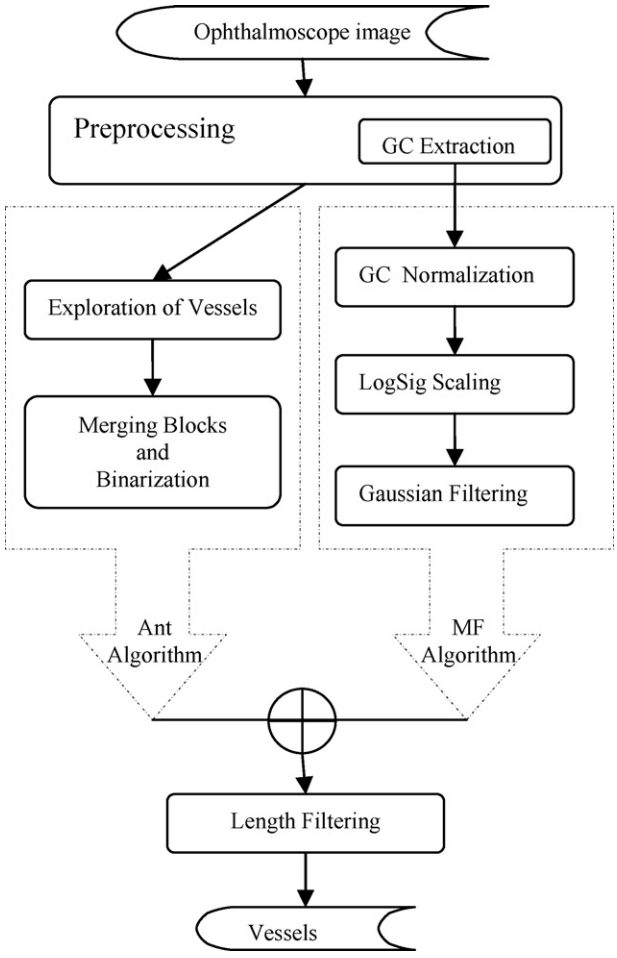

Fig. 1 – Proposed system architecture.

MF filter K is then normalized as in Eq. (9)

$$K_i'(x,y) = K(x,y) - \frac{1}{(\#\text{of point in } N)} \sum_{\tilde{p}_i \in N} K_i(x,y) \tag{9}$$

The MF kernels K_i' (where i indicates rotated K kernel, in MF applications, it is generally equal to 12.) are convolved with the green channel of retinal image. The output image is constructed as the maximum responses from the 12 resultant images.

3. Proposed MF/ant algorithm

In this section, proposed ant algorithm is introduced. It comprises the following steps (Fig. 1):

- *Preprocessing step*: In this stage, preprocessing is done over the raw input ophthalmoscope image (i.e. retinal image). This module includes sub-processing modules as; Green Channel Extraction, Image Enhancement, and Block Marking Processing.
- *Ant algorithm step*: This step is parallelized with the MF algorithm step. The processed image (gray level enhanced retinal image) is passed through the sub-steps of the follow-

Fig. 2 – (a) Original ophthalmoscope image, (b) green channel of the original ophthalmoscope image, (c) nonlinear intensity transformed form of (b).

ings: Exploration of vessels using Marked Blocks, Merging Blocks and Binarization.

- *MF algorithm step*: Second parallel step of the proposed approach. This step includes the sub-steps of Green Channel Normalization, LogSig Scaling and Gaussian Filtering to find vessels.
- *Merging step*: ant algorithm Result is combined with MF Result to produce almost the resultant image.
- *Length filtering step*: The final process of the proposed system

The following section described the steps given above in detail.

3.1. *Preprocessing*

In preprocessing step, following operations are applied on original retinal images sequentially;

- Conrast between vessels and background is very distinctive in *green channel* of the colored ophthalmoscope images [34]. Therefore, "G" component of the RGB retinal image is extracted.(Fig. 2b)
- Additional enhancement over the extracted image is implied through the *nonlinear intensity transformation*. [i.e. in Matlab, imadjust tool is used for transforming image levels {min, max} into {0,255} range with gamma = 1] (Fig. 2c).
- According the probability distribution function of the blood vessels widths, the observed maximum value of the vessel width is less then 15 pixels on the ophthalmoscope images in the size of 512×512 [35]. From this inspiration, the image is divided into *small sized of blocks* in the implementation.
- Divided blocks of the image are checked to validate whether or not the block contains part of vessel. Validation is supplied by controlling intensity entropy on the small sized block. If the entropy has small value, this block does not carry vessel part (i.e. flat surface, having almost the same value) so it is not marked. If the entropy shows some degree of nonstability, *the block is marked*. The marked blocks are used for ant distribution in the next stage of the algorithm.

Table 1 – Determined suitable parameters for ant algorithm.

Parameter	Value
β	5.0*
q_0	0.95*
ρ	0.3*
θ	200
ψ	0.4
Number of iteration	10

* Standard values of the ant algorithm parameters in [32].

3.2. Ant algorithm

The ant algorithm is applied to the blocks previously marked by preprocessing step.

Each block is considered as a two-dimensional graph where the image pixels are assumed as vertices. In classical ant algorithms, optimal tour search of the ant depends on the edges over the paths. Since the graphs of retinal image blocks are used, the edges indicate only the connectivity information of the pixels.

At initialization, pheromones on each pixel are initialized with very small values such as 10^{-10}. Other tunable parameters explained in Section 2.1 are also initialized with suitable values in Table 1.

So the proposed ant algorithm implies the following sub-steps;

Exploration of vessels: At each iteration, ants are located on uniformly distributed random pixels. Then they traverse pixels step by step. At each step, the next suitable neighbor pixel is selected according to ACS state transition rule in Eq. (2) where the heuristic function η_{ij} as defined by the Eq. (10).

$$\eta_{ij} = \begin{cases} \dfrac{P_{max} - P_{ij}}{P_{max}} & \text{if } P_{ij} < \theta \text{ and } P_{ij}/P_{max} > \psi \\ 0 & \text{otherwise} \end{cases} \quad (10)$$

In Eq. (10) P_{max} is the maximum gray level value in marked block. P_{ij} is the gray value of pixel(i,j). θ is the constant threshold and ψ is the contrast ratio.

Heuristic function η_{ij} attracts ants to the pixels belong the blood vessels. If there is no suitable pixel to traverse, the ant dies (Fig. 3). Another reason of dying the ant is the limited usage of memory. Every ant has limited memory in the size of traversed edge number. The size of the memory is discussed in experimental results section of this paper. After ants complete their strolls, pheromone levels are updated by the Eq. (11):

$$\tau_{ij}(\text{new}) = (1-\rho)\tau_{ij}(\text{old}) + \sum_{k=1}^{m} \Delta\tau_{i,j}^{k} \quad (11)$$

where m is the number of ant and $\Delta\tau_{i,j}^{k} = \eta_{ij}$.

After the update phase, single cycle of the algorithm is completed. This cycle is repeated by the predefined number of iterations (Table 1).

Consequently, the amount of pheromone deposited on each pixel gives the intensity level of that pixel.

Merging blocks and binarization: For generating binary image, indicating the presence of blood vessels, thresholding over pheromone levels are applied.

Thresholding is determined by the accuracy measurement (determination details are handled in Section 3.2). The observed maximum accuracy level is set as threshold value used for binarization.

3.3. Proposed MF application

In this section, GC gray image extracted in preprocessing step is taken as input into our modified MF algorithm.

This approach is described in the following sub-steps:

GC normalization: The images in the database have different illumination conditions. This variation affects the sensitivity and segmentation performance of the MF. In order to get rid of the negative effects of the variation, normalization is applied on images by Eq. (12).

$$GC'(x,y) = \frac{GC(x,y) - \mu_{gc}}{\sigma_{gc}} \quad (12)$$

LogSig scaling: The LogSig-function is well known and used, e.g., to realize Multilayered Perceptron neural networks. LogSig is used for data pre-treatment in analysis methods, where it takes care of the two major steps: elimination of the influence of the outliers, and scaling of data [36]. In this paper, LogSig is used for eliminating outliers after normalization step.

The LogSig-approach is almost identical to the fuzzification of variables with sigmoid shaped activation function. One of the strengths of Fuzzy logic is to provide understandable means to the user to incorporate his domain knowledge to data analysis. The LogSig-based pre-treatment of data offers the same advantages when studying data with other algorithms than fuzzy inference. This LogSig-approach use S-shaped function to scale the data. The advantage of this is to eliminate the influence of outliers [36]. LogSig is given as in

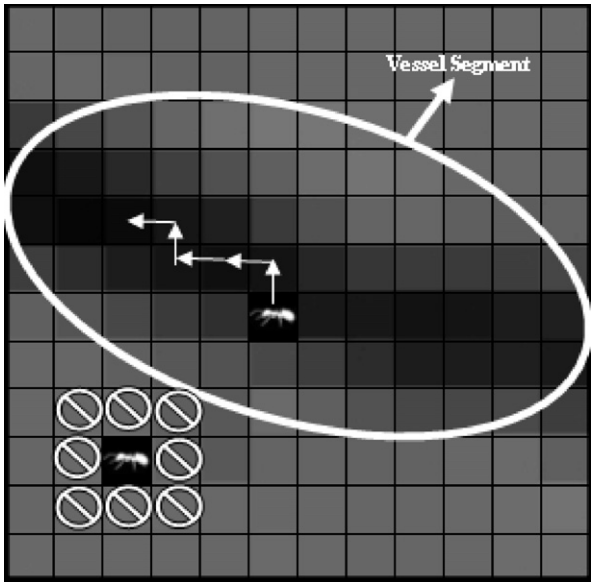

Fig. 3 – Traverse of the ant (middle) and dying of ant (left-bottom).

Table 2 – Accuracy results for the first retinal image of the DRIVE under the parameters of the proposed ant algorithm.

Blocking size	Number of ants	Ant memory			
		10 Maximum accuracy (time)	20 Maximum accuracy (time)	50 Maximum accuracy (time)	100 Maximum accuracy (time)
5 × 5	5	0.924 (25 s)	0.9243 (26 s)	0.9244 (27 s)	0.9249 (27 s)
	10	0.9271 (45 s)	0.9264 (46 s)	0.9276 (47 s)	0.9266 (47 s)
	20	0.9285 (83 s)	0.9284 (88 s)	0.9284 (88 s)	0.9291 (88 s)
	100	0.9288 (425 s)	0.9289 (428 s)	0.9291 (430 s)	0.9290 (430 s)
12 × 12	5	0.9037 (12 s)	0.9092 (17 s)	0.9139 (19 s)	0.9130 (21 s)
	10	0.9042 (19 s)	0.9130 (27 s)	0.9208 (32 s)	0.9181 (37 s)
	20	0.9078 (38 s)	0.9155 (47 s)	0.9214 (66 s)	0.9201 (70 s)
	100	0.9114 (150 s)	0.9174 (232 s)	0.9221 (330 s)	0.9258 (341 s)
24 × 24	5	0.887 (6 s)	0.8892 (8 s)	0.8939 (11 s)	0.8947 (12 s)
	10	0.8918 (9 s)	0.8961 (12 s)	0.9015 (19 s)	0.9053 (24 s)
	20	0.8953 (13 s)	0.9004 (19 s)	0.9072 (32 s)	0.9075 (44 s)
	100	0.9025 (48 s)	0.9062 (82 s)	0.91 (145 s)	0.9214 (217 s)

Eq. (13). In this equation, "c" indicates center of nominal range, "r" indicates radius of the nominal range. In most applications (c,r) is accepted as (0,1).

$$GC''(x,y) = \frac{1}{1+\exp^{-2(GC'(x,y)-c)/r}} \quad (13)$$

Gaussian filtering: There are some other alternatives for applying frequency domain filters for MF. Most popular filter designs for MF are Gaussian, Chebychev and Kaiser.

In brief, we have tested these three kernels on 20 ophthalmoscope images of DRIVE database. We have obtained best results with 13 point-Gaussian kernel with $L = 9$ and standard deviation $\sigma = 2$. (We do not use the kernel values in [37,38]. Please refer to Section 4.3 of this paper)

As indicated in Eqs. (8) and (9), the Gaussian is applied with 10° rotation. Since we have used 10°, 18 kernels are applied for edge enhancement. You can see one of them in Fig. 4.

Length filtering: The binary images taken from proposed ant and proposed MF algorithm are merged together to form the resultant binary image. This merging is accomplished through the classic OR operator.

After the merging stage is passed, the binary output image is obtained. Since this image contains some unwanted ledges and disconnected small vessel parts, length filtering is needed.

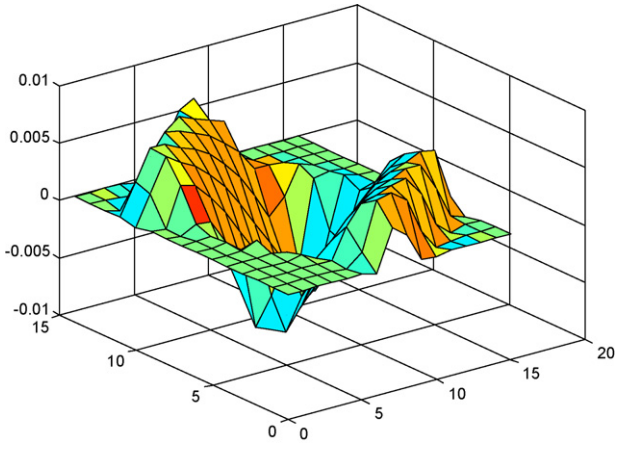

Fig. 4 – Applied Gaussian filter with $\theta = 50°$ rotated.

On the binary image, 8-connected component analysis is done. Every isolated part is labeled as an object. Each object is entered into a LUT table with its label and length information.

LUT table is sorted according to the length information in descending order. We applied a threshold length value to LUT. So the unwanted and disconnected small vessel particles are cleared from the binary image. The result is pure and ready for landmark point extraction module.

4. Experimental results

4.1. *Materials*

The proposed algorithms in this work were tested on DRIVE database images (for standard comparison with early works). DRIVE database contains 40 TIFF formatted RGB retinal images with a size of 565 × 584 pixels. The images are handled into two sets: Training and testing. The database contains hand labeled retina images created by two human observers (pathologists) as well. They are used for comparison with the images acquired from training set. Although both of them used in comparisons, only the First observer's performance is accepted as Gold Standard (selection of the first pathologist as Gold standard is used in literature).

The comparison performances of the algorithms are measured using area under ROC curves and maximum segmentation accuracy.

ROC curve represents the variation of false ratio versus true ratio on different threshold values. True ratio is calculated by dividing true pixels of the vessels by the number of pixels in fist observer hand labeled retinal image (denoted by Gold Standard) and false ratio is calculated by dividing false pixels by the number of nonvessels pixels in Gold Standard image. If the area under ROC curve is equal to "1", this means perfect matching of the algorithm result with Gold Standard. The efficient algorithm is the one having the ROC curve area closest to "1".

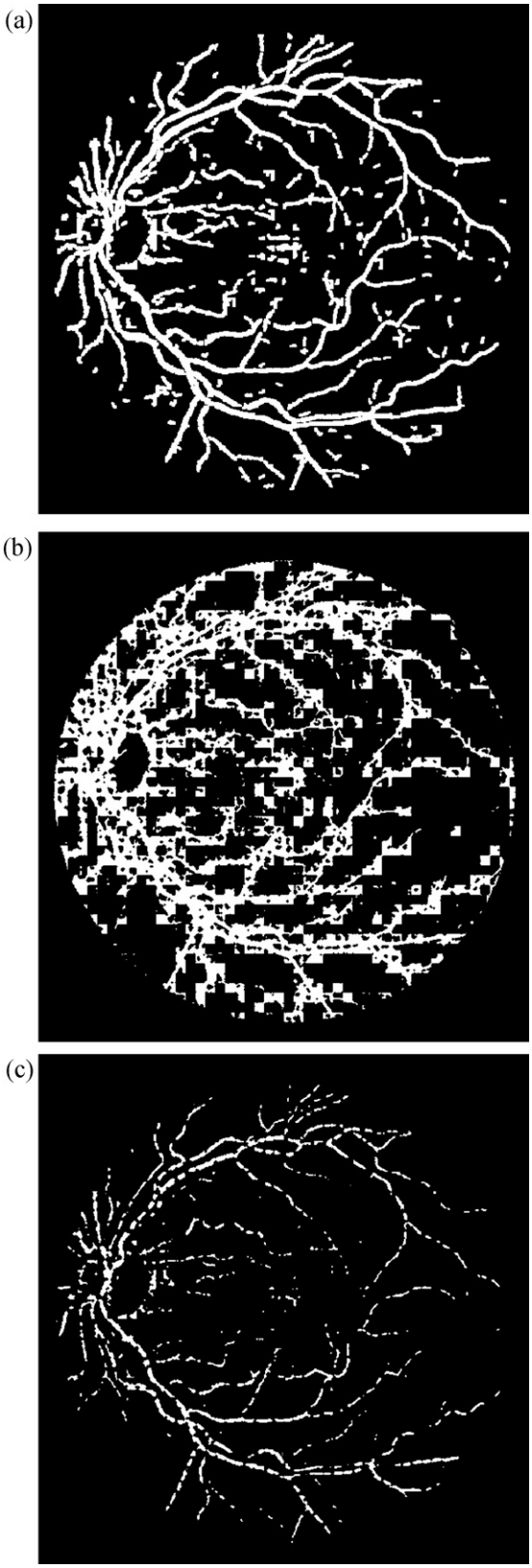

Fig. 5 – Segmentation results with different q_0 and ρ parameters. (a) Result with parameters in Table 1. (b and c) Segmentation results with $q_0 = 0.2$, $\rho = 0.1$ and $q_0 = 0.7$, $\rho = 0.9$, respectively.

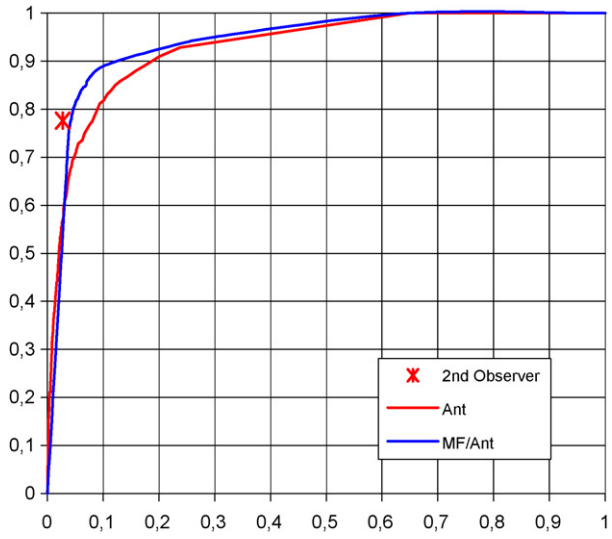

Fig. 6 – ROC curves for the first image of DRIVE.

Maximum accuracy indicates how to extract a binary image that matches to a high degree the vessel mages. It is estimated by the maximum ratio of the total number of truly classified pixels by the number of pixels in field of view (FOV).

4.2. *Parameters setting*

There are two types of parameters to be set efficiently: parameters of ant and MF algorithms.

It is really hard to assign best values for the parameters of the ant algorithm. Therefore, the convenient ant algorithm parameters are determined by the experiments carried out on the retinal images of DRIVE database through the accuracy calculations. Determined parameters are listed in Table 1. Fig. 5 shows segmentation results of the ant algorithm with different settings of "q_0" and "ρ" parameters (without combination of matching filter).

On the other hand, ant algorithm parameters affecting the algorithm performance like number of ants and used ant memory are directly correlated with the varying blocking size. The maximum accuracy results are shown in Table 2 with respect to the affecting parameters. They are obtained from single retinal image.

Table 2 indicates that number of ants and their memories should be balanced. The tests with small number of ants with large memories and large number of ants with short memories deduced that they decrease the performance of segmentation. In the view of the Table 2, we prefer to use 12×12 block size with 10 ants and memory size of 50. This combination gives the accuracy of 0.9208.

Although the maximum accuracy results are observed on the usage of 5×5 block size, this size of block cannot behave correctly inside the thicker vessel segments. When the block falls on the vessel having the width greater than 5 pixels, the inner side of the vessel can be marked as background. Since we do not want to double border extraction for vessel segment, we do not use 5×5 blocks.

Table 3 – The areas under ROC curves for each DRIVE image and their averages.

Image number	Area under ROC curve	
	Ant algorithm	MF/ant algorithm
1	0.9463	0.9546
2	0.9459	0.9528
3	0.9323	0.9410
4	0.9344	0.9387
5	0.9309	0.9385
6	0.9278	0.9357
7	0.9191	0.9275
8	0.9111	0.9299
9	0.9233	0.9286
10	0.9274	0.9361
11	0.9237	0.9376
12	0.9428	0.9488
13	0.9199	0.9277
14	0.9417	0.9490
15	0.9382	0.9468
16	0.9344	0.9357
17	0.9209	0.9367
18	0.9394	0.9492
19	0.9403	0.9509
20	0.9421	0.9493
Average	0.9320	0.9407

Table 4 – Determining the average threshold and maximum accuracy average (MAA) for proposed methods.

Image number	Threshold	Maximum accuracy	
		Ant algorithm	MF/ant algorithm
1	10.4	0.9120	0.9323
2	10.9	0.9115	0.9370
3	9.6	0.9118	0.9207
4	9.3	0.9239	0.9368
5	9.4	0.9205	0.9238
6	10.4	0.9208	0.9264
7	7.9	0.9234	0.9269
8	8.6	0.9124	0.9145
9	8.9	0.9309	0.9386
10	8.5	0.9290	0.9341
11	10.5	0.9160	0.9196
12	8.7	0.9233	0.9272
13	9.2	0.9187	0.9267
14	9	0.9213	0.9259
15	12.3	0.9294	0.9219
16	8.1	0.9168	0.9293
17	11.6	0.9169	0.9342
18	11.5	0.9155	0.9354
19	9	0.9208	0.9288
20	9.6	0.9282	0.9365
Average	9.67	0.9202	0.9293

For proposed MF algorithm, we examine length and prolate parameter of Gaussian kernel. In this parameter tuning, we have used retinal images of DRIVE database too. Length sizes are tested incrementally from 6 points to 25 points. We observed that the comparison of retinal image with hand labeled image has the maximum PSNR measurement on the 13 points. So we have chosen the length of Gaussian as 13 points. When we construct the spheroid form of the Gaussian we take $L = 9$ [2]. The prolate of the Gaussian is tested with σ parameter. The maximum PSNR measurement has shown $\sigma = 2$.

In this paper, Gaussian rotation angle θ is set 10°. In other words, we have 18 kernels to construct maximum response image. This modification is done to catch the capillaries. When the registration process requires more landmark points, capillaries are getting more important.

The response image is than binarized with the local entropy thresholding [15].

4.3. *Experiments on DRIVE database*

Experiments are applied on 20 DRIVE test images for both ant algorithm and MF/ant algorithm. For all experiments, the ant algorithm parameters are set as in Table 1 and blocking size is chosen as 12×12 with $n = 10$ (number of ants) and $m = 50$ (ant memory).

The ROC curves for each image are obtained by manually thresholding the image with the pheromone values starting from 10^{-10} level (initial pheromone value) up to 100 in step size of 0.1.

As an example, Fig. 6 compares the ROC curves of ant, MF/ant (our proposed method) and second human observer performance which provide only one true/false fraction pair on the first Gold Standard image.

Like the example given in Fig. 6, all ROC curves of 20 images of DRIVE are figured out. The areas under the ROC curves for both ant and our MF/ant are listed in Table 3. As can be seen

Table 5 – A comparison of different MF methods with proposed MF/ant algorithms.

Vessel detection method	Average ROC area	Maximum accuracy average (MAA)	Execution time (s)
MF/ant (this work)	0.9407	0.9293	35
Ant (this work)	0.9320	0.9202	32
GMF* [2]	0.7550	0.8850	2
Staal et al.	0.9587	0.9547	900
Kirsch [40]	0.8687	0.8939	0.642
Sobel operator	0.7571	0.8936	0.264
Prewitt operator	0.7486	0.8951	0.281
Zana and Klein [35]	0.9174	0.9439	NaN

* GMF is general MF algorithm. Some works indicate it as MF only.

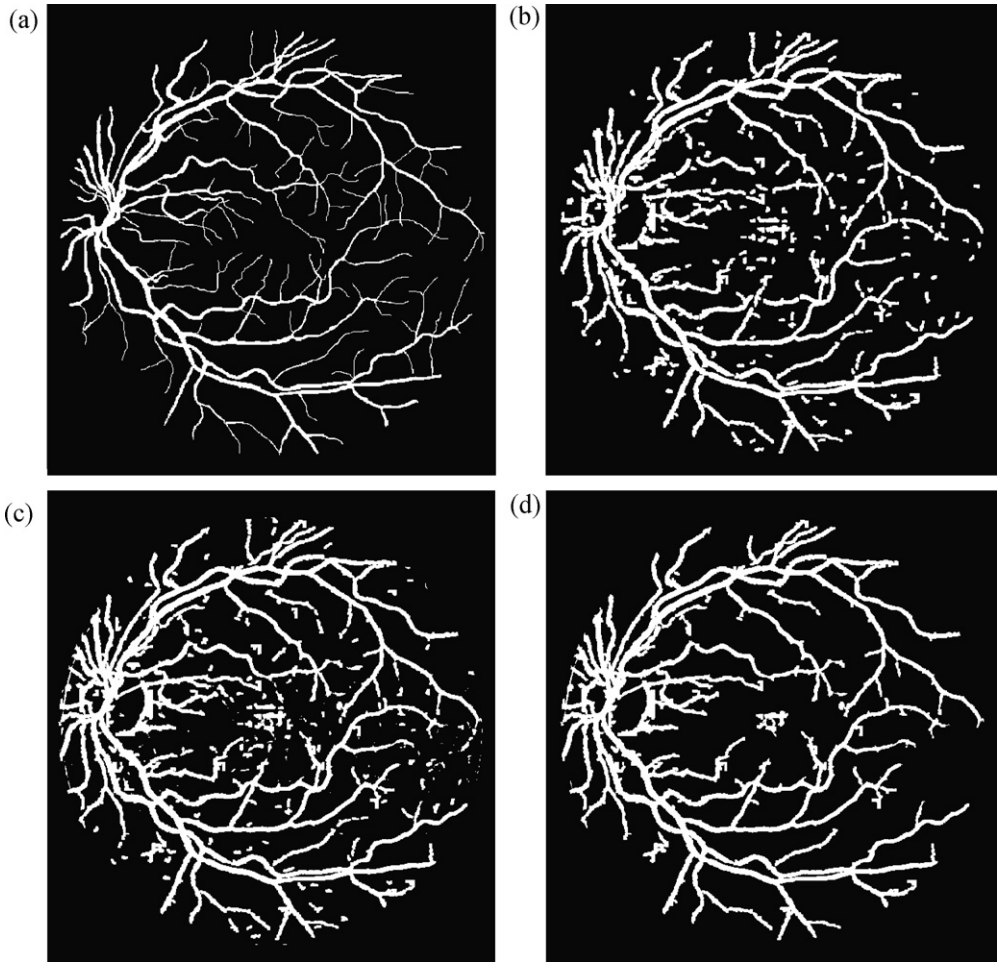

Fig. 7 – (a) Gold standard, (b) ant output, (c) our MF/ant output, (d) our MF/ant algorithm with length filtering.

from the results, MF/ant approach improves the efficiency of ant algorithm application.

In Table 4 Our second experiment is applied for finding the best thresholds under the circumstances of maximum accuracies. Again, thresholds are applied in the range of 10^{-10} to 100 manually. MA values set the best thresholds. The results are indicated in Table 4. According to the table, average threshold value is suggested to use for binarization purpose in general.

In Table 5, our proposed algorithm is compared with the other MF based methods in literature. In previous works [37,38], OGMF (Optimized GMF) and GAMF (Genetically Optimized GMF), are indicated having the performances as 0.9246/0.9287 and 0.9582/0.9420 for ROC/MAA analysis respectively. They seem to compete with other results in Table 5. We have not embedded their results in table, because there is a serious problem related with L parameter. In OGMF and GAMF methods, L is taken as floating number (i.e. $L = 13.4086$). Since "L" is the parameter of vessel length in pixels, it is not possible to take it in precision of floating number. So we have not included OGMF and GAMF here. Although Staal et al.'s method [39] seems to be better than our approach, it suffers from higher computational complexity to find vessels.

5. Discussion and conclusion

In this paper, a novel hybrid model of matched filter and ant-based algorithm (MF/ant algorithm) is proposed for blood vessels segmentation. The performance of MF/ant algorithm is shown by ROC curve analysis and accuracy measurement on DRIVE database images.

Experiments show that ant-based approach increases the accuracy of the match filters. In order to improve our performance, we should take care of the following concepts:

a. The vessel segments in our resulted binary images are thicker than vessels in gold standard images. Since the thicker vessels are directly involved in measurement, the accuracy and the area under ROC curves are affected by false positive calculations. This decreases the segmentation performances.
b. The virtual ants mistakenly trace over pathological areas assumed as probable vessel segments (the central area of the Fig. 2). Fig. 7a shows the gold standard image for Fig. 2. Fig. 7b represents ant result. Fig. 7.c indicates our MF/ant result. Both (b,c) figures are obtained without length filtering. The final image shows the result of MF/ant algorithm

with length filtering. As can be seen from the final image, MF/ant extracts vessels perfectly but pathological area can affect the result.

We aim to get rid of pathological areas in the future work. In order to achieve this goal, we are going to use chromaticity channel extraction.

REFERENCES

[1] A. Hoover, V. Kouznetsova, M. Goldbaum, Locating blood vessels in retinal images by piecewise threshold probing of a matched filter response, IEEE Trans. Med. Imaging 19 (3) (2000) 203–210.

[2] S. Chaudhuri, S. Chatterjee, N. Katz, et al., Detection of blood vessels in retinal images using two-dimensional matched filters, IEEE Trans. Med. Imaging 8 (3) (1989) 263–269.

[3] R. Nekovei, Y. Sun, Back-propagation network and its configuration for blood vessel detection in angiograms, IEEE Trans. Neural Networks 6 (1) (1995) 64–72.

[4] B. Cote, W. Hart, M. Goldbaum, P. Kube, M. Nelson, Classification of blood vessels in ocular fundus images, Computer Science and Engineering Department, University of California, San Diego, Tech Report, 1994.

[5] S. Tamura, K. Tanaka, S. Ohmori, K. Okazaki, A. Okada, M. Hoshi, Semiautomatic leakage analyzing system for time series fluorescein ocular fundus angiography, Pattern Recognit. 16 (2) (1983) 149–162.

[6] M.E. Martinez-Perez, A.D. Hughes, A.V. Stanton, S.A. Thom, A.A. Bharath, K.H. Parker, Segmentation of retinal blood vessels based on the second directional derivative and region growing, Proc. ICIP (1999) 173–176.

[7] O. Chutatape, L. Zheng, S.M. Krishnan, Retinal blood vessel detection and tracking by matched Gaussian and Kalman filters, in: Proc. of 20th Annu. Int. Conf. IEEE Eng Med. Biol., 1998, pp. 3144–3149.

[8] Y. Tolias, S.M. Panas, A fuzzy vessel tracking algorithm for retinal images based on fuzzy clustering, IEEE Trans. Med. Imag. 17 (2) (1998) 263–273, Apr.

[9] A. Can, H. Shen, J.N. Turner, H.L. Tanenbaum, B. Roysam, Rapid automated tracing and feature extraction from retinal fundus images using direct exploratory algorithms, IEEE Trans. Inf. Technol. Biomed. 3 (2) (1999) 125–138.

[10] H. Nezamabadi-pour, S. Saryazdi, E. Rashedi, Edge detection using ant algorithms, Soft Comput. 10 (2006) 623–628.

[11] D.-S. Lu, C.-C. Chen, Edge detection improvement by ant colony optimization, Pattern Recognit. Lett. 29 (4) (2008) 416–425.

[12] Y.-C. Liang, A.H.-L. Chen, C.-C. Chyu, Application of a hybrid ant colony optimization for the multilevel thresholding in image processing, in: ICONIP'06, Part II, LNCS, vol. 4233, 2006, pp. 1183–1192.

[13] A.R. Malisia, H.R. Tizhoosh, Image thresholding using ant colony optimization, crv, in: The 3rd Canadian Conference on Computer and Robot Vision (CRV'06), 2006, p. 26.

[14] X. Zhao, M.-E. Lee, S.-H. Kim, Improved image thresholding using ant colony optimization algorithm, Int. Conf. Adv. Lang. Process. Web Inf. Technol. (2008) 210–215.

[15] A.R. Malisia, H.R. Tizhoosh, Applying ant colony optimization to binary thresholding, IEEE Int. Conf. Image Process. (2006) 2409–2412.

[16] J. Handl, B. Meyer, Ant-based and swarm-based clustering, Swarm Intell. 1 (2007) 95–113.

[17] E. Lumer, B. Faieta, Diversity and adaptation in populations of clustering ants, in: From Animals to Animats 3: Proceedings of the Third International Conference on Simulation of Adaptive Behavior, 1994, pp. 501–508.

[18] J. Handl, J. Knowles, M. Dorigo, Ant-based clustering and topographic mapping, Artif. Life 12 (1) (2006) 35–61.

[19] Q. Li, Z. Shi, J. Shi, Z. Shi, Swarm intelligence clustering algorithm based on attractor, in: L. Wang, K. Chen, Y.-S. Ong (Eds.), Lecture Notes in Computer Science: vol. 3612. Advances in Natural Computation, First International Conference, ICNC, 2005, pp. 496–504.

[20] S. Ouadfel, M. Batouche, AntClust: an ant algorithm for swarm based image clustering, Inf. Technol. J. 6 (2) (2007) 196–201.

[21] X.-N. Wang, Y.-J. Feng, Z.-R. Feng, Ant colony optimization for image segmentation, in: Proc. of the Fourth International Conf. on Mach. Learn. and Cyber, Guangzhou, 2005, pp. 5355–5360.

[22] R. Laptik, D. Navakauskas, Application of ant colony optimization for image segmentation, Electron. Electrical Eng. 8 (80) (2007) 13–18.

[23] S. Saatchi, C.C. Hung, Hybridization of the ant colony optimization with the k-means algorithm for clustering, Lecture Notes Comput. Sci. 3540 (2005).

[24] B. Zhao, Z. Zhu, E. Mao, Z. Song, Image segmentation based on ant colony optimization and K-means clustering, in: Porc. of Int. Conf. Automat. Logistics, 2007, pp. 459–463.

[25] Y. Weili, G. Lei, Z. Tianyun, X. Guchu, Image segmentation method by combining watersheds and ant colony clustering, Proc. Control Conf. (2007) 526–529.

[26] M. Dorigo, V. Maniezzo, A. Colorni, Positive feedback as a search strategy, Technical Report, Dipartimento di Elettronica, Politecnico di Milano, Milano, Italy, 1991.

[27] M. Dorigo, Ottimizzazione, Apprendimento Automatico, ed Algoritmi Basati su Metafora Naturale, PhD thesis, Politecnico di Milano, 1992.

[28] M. Dorigo, V. Maniezzo, A. Colorni, The ant system: optimization by a colony of cooperating agents, IEEE Trans. Syst. Man Cybern. Part B 26 (1996) 29–41.

[29] M. Dorigo, G. Di Caro, Ant colony optimization: a new metaheuristic, Proc. Congr. Evol. Comput. 2 (1999) 1470–1477.

[30] M. Dorigo, M. Birattari, T. Stützle, Ant colony optimization: artificial ants as a computational intelligence technique, IEEE Comput. Intell. Mag. (1999) 28–38.

[31] E. Bonabeau, M. Dorigo, G. Theraulaz, Swarm Intelligence From Natural to Artificial Systems, Oxford University Press, New York, NY, 1999.

[32] M. Dorigo, L.M. Gambardella, Ant colony system: a cooperative learning approach to the traveling salesman problem, IEEE Trans. Evol. Comput. 1 (1997) 53–66.

[33] M. Dorigo, L.M. Gambardella, Ant colonies for the traveling salesman problem, Bio Syst. 43 (1997) 73–81.

[34] R. Perfetti, E. Ricci, D. Casali, G. Costantini, Cellular neural networks with virtual template expansion for retinal vessel segmentation, IEEE Trans. Circuits Syst. 54 (2) (2007) 141–146.

[35] F. Zana, J.C. Klein, A multimodal registration algorithm of eye fundus images using vessels detection and Hough transform, IEEE Trans. Med. Imaging 18 (5) (1999) 419–428.

[36] K. Hätönen, S. Laine, T. Similä, Using the LogSig function to integrate expert knowledge to self-organizing map (SOM) based analysis, in: IEEE Int. Workshop Soft Comput. Ind. Appl. (SMCia/03), 2003, pp. 145–150.

[37] M. Al-Rawi, M. Qutaishat, M. Arrar, An improvement matched filter for blood vessel detecetion of digital retinal images, Comput. Biol. Med. 37 (2007) 262–267.

[38] M. Al-Rawi, H. Karajeh, Genetic algorithm matched filter optimization for automated detection of blood vessels from digital retinal images, Comput. Methods Programs Biomed. 87 (2007) 248–253.

[39] J. Staal, B. Ginneken, M. Niemeijer, A. Viegever, M.D. Abramoff, Ridge based vessel segmentation in color images of retina, IEEE Trans. Med. Imaging 23-4 (2004) 501–509.

[40] H. Li, O. Chutatape, Fundus image feature extraction, in: Proceeding of the 22nd IEEE Conference on Engineering in Medicine and Biology Society, vol. 1, 2000, pp. 3071–3073.